INTERFACE FOCUS

rsfs.royalsocietypublishing.org

Research

Cite this article: Gruson H, Andraud C, Daney de Marcillac W, Berthier S, Elias M, Gomez D. 2018 Quantitative characterization of iridescent colours in biological studies: a novel method using optical theory. *Interface Focus* **9**: 20180049.
http://dx.doi.org/10.1098/rsfs.2018.0049

Accepted: 11 October 2018

One contribution of 11 to a theme issue 'Living light: optics, ecology and design principles of natural photonic structures'.

Subject Areas:
biomaterials, biophysics, environmental science

Keywords:
iridescence, structural colours, thin-film interferences, hummingbirds, Lepidoptera, visual signals

Author for correspondence:
Hugo Gruson
e-mail: hugo.gruson@normalesup.org

Electronic supplementary material is available online at https://dx.doi.org/10.6084/m9.figshare.c.4275911.

THE ROYAL SOCIETY PUBLISHING

Quantitative characterization of iridescent colours in biological studies: a novel method using optical theory

Hugo Gruson[1], Christine Andraud[2], Willy Daney de Marcillac[3], Serge Berthier[3], Marianne Elias[4] and Doris Gomez[1,3]

[1]CEFE, Univ Montpellier, CNRS, Univ Paul Valéry Montpellier 3, EPHE, IRD, Montpellier, France
[2]CRC, MNHN, Ministère de la Culture et de la Communication, CNRS, Paris, France
[3]INSP, Sorbonne Université, CNRS, Paris, France
[4]ISYEB, CNRS, MNHN, EPHE, Sorbonne Université, Paris, France

HG, 0000-0002-4094-1476; ME, 0000-0002-1250-2353; DG, 0000-0002-9144-3426

Iridescent colours are colours that change with viewing or illumination geometry. While they are widespread in many living organisms, most evolutionary studies on iridescence do not take into account their full complexity. Few studies try to precisely characterize what makes iridescent colours special: their angular dependency. Yet, it is likely that this angular dependency has biological functions and is therefore submitted to evolutionary pressures. For this reason, evolutionary biologists need a repeatable method to measure iridescent colours as well as variables to precisely quantify the angular dependency. In this study, we use a theoretical approach to propose five variables that allow one to fully describe iridescent colours at every angle combination. Based on the results, we propose a new measurement protocol and statistical method to reliably characterize iridescence while minimizing the required number of time-consuming measurements. We use hummingbird iridescent feathers and butterfly iridescent wings as test cases to demonstrate the strengths of this new method. We show that our method is precise enough to be potentially used at intraspecific level while being also time-efficient enough to encompass large taxonomic scales.

1. Introduction

Most interactions between organisms, whether between different species (interspecific) or different individuals of the same species (intraspecific), involve communication. Communication can have different purposes (e.g. warning, camouflage, display) and use different channels (e.g. olfactory, acoustic, visual) [1]. In particular, colour is a specific kind of communication channel that can be produced through two non-mutually exclusive mechanisms: pigmentary colours are generated by the selective absorption of some wavelengths by special molecules called pigments while structural colours are generated by the physical interaction of light with matter, causing dispersion, diffraction or interferences [2].

Among structural colours, iridescent colours change depending on the illumination or observation angle. They can be produced by interferences of light after reflection by a thin-film or multilayer structure, or diffraction on a grating. Iridescent colours are present in many taxa, and particularly widespread among bony fishes (Actinopterygii), insects, as well as some birds (see detailed review in table 1 for studies on each one of these taxa). Iridescent colours seem to be involved in many important biological processes [123] and their angular dependency is likely under selection to produce complex visual signals [74,87,115,124]. In some cases, however, angular dependency may be selected against [125]. In all those cases, the study of the evolution of iridescent colours requires a precise quantification of the angular dependency. However, the inherent physical complexity of iridescent colours has hampered the development of quantitative methods to fully describe them in the angle space.

Table 1. Review of the methods used in the literature to study iridescent colours from multilayer or thin-film structures. The criteria we used for studies to be included in the table were the following: (i) at least one quantitative reflectance measurement using a spectrometer, (ii) functioning with white light (no monochromatic illumination), and (iii) the patch measured had to be described as iridescent in the article. A more detailed version of this table, with all angle configurations and colour variables used for each study is available in the electronic supplementary material. The terms 'constant illumination', 'constant collection', 'constant angle bisector' and 'constant span' are defined in figure 3*d*.

no. measurements	fibre configuration (no. studies)	birds	arthropods	others
single measurement	single fixed angle (53)	[3–33]	[34–48]	bony fishes [49]; mammals [50]; plants [51–54]
	single measurement relative to the structure orientation (6)	—	[55–60]	—
multiple measurements along a single line	constant illumination (5)	[61]	[62–64]	bacteria [65]
	constant collection (2)	[66]	[67]	—
	constant angle bisector (16)	[68–78]	[79–83]	—
	constant span (16)	[84–87]	[88–96]	bony fishes [97]; lizards [98,99]
multiple measurement lines	multiple constant illuminations (4)	[100]	[101,102]	bacteria [103]
	multiple constant collections (1)	[104]	—	
	multiple constant spans (1)	[105]	—	
	constant illumination and bisector (3)	—	[106,107]	bacteria [108]
	multiple illumination and bisector (1)	—	[109]	—
	constant illumination and span (3)	[110,111]	[112]	—
	constant span and bisector (6)	[113–115]	[116–118]	gastropods [119]
	constant illumination, span and bisector (4)	[120,121]	[102,122]	—

We reviewed all studies that performed reflectance measurements of biological samples with iridescent colours produced by a multilayer or a thin-film structure in table 1. We notice two main trends: (i) many studies measure iridescence at a single fixed angle (first row in table 1). In these studies, authors generally remain cautious and warn they are not attempting to measure angle dependency. However, the multilayer or thin film producing iridescent colours may not be parallel to the sample surface [67,80,96,102,109], and the angle between them and the sample surface may vary between species or even between individuals of the same species [105]. Hence, even though the angle of the measuring optical fibres relative to the macroscopic is constant, the angle relative to the structures is not. This jeopardizes any biological interpretation of differences between samples because the effects of many different parameters are intertwined.

(ii) Other studies take measurements at multiple angles but few attempt to precisely quantify angle dependency ('Literature review' folder in electronic supplementary material). Even when angle dependency is quantified, variables never stem from a theoretical approach, which leads to a large diversity of custom variables for each author. This heterogeneity in the methods, variable naming and sign conventions has likely hindered the spread of new concepts and results among researchers working on iridescence in living organisms.

Osorio & Ham [110] and Meadows *et al.* [114] started to address this heterogeneity in measurement methods and advocated for the use of a goniometer to reliably measure colour in a controlled angle configuration. However, they did not propose a detailed protocol or statistical tools to study angular dependency. Here, we use the optical laws that govern iridescence to propose a set of parameters to characterize angle dependency of brightness, hue and saturation of iridescent colours. Next, we confirm the validity of these equations for complex biological structures using two highly different groups of organisms well known for their iridescent colours: Trochilidae (hummingbirds) and Lepidoptera (i.e. butterflies and moths), including the iconic *Morpho* butterflies that harbour large wings with bright iridescent blue colours. The standard framework we propose here makes iridescent colours comparable across taxa and across studies, opening up new perspectives in the study of their biological functions.

2. Model

2.1. Choice of colour variables

Since we want to produce a general method that would not depend on any specific vision system, we use variables directly derived from spectra, without computing vision models. We define brightness B as the average reflectance over a range between the minimal (λ_{min}) and maximal (λ_{max}) wavelengths (B_2 in Montgomerie [126]), saturation S as the full width at half maximum reflectance and hue H as the wavelength at which reflectance is maximal (H_1 in Montgomerie [126]). These three variables are represented in figure 1 and are the most common measures of brightness, hue and saturation in studies about iridescence (see the literature review in the electronic supplementary material).

2.2. Assumptions and equations

Our method relies on three assumptions that greatly simplify the equations for brightness, hue and saturation in the angle

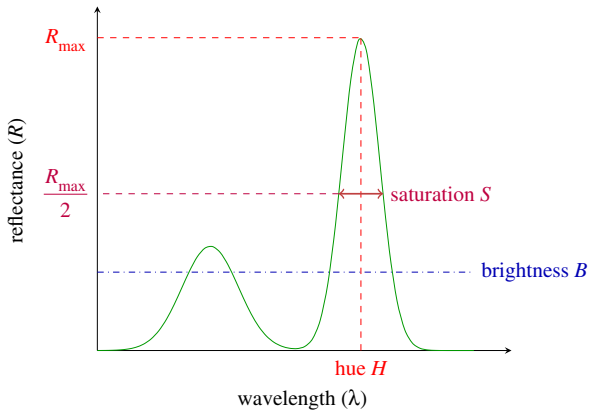

Figure 1. Graphical representation of the variables we used for hue H (wavelength at peak reflectance R_{max}; called H_1 in Montgomerie [126]), brightness B (average of reflectance over the wavelength range of interest; B_2 in Montgomerie [126]) and saturation S (full width at half maximum; no equivalent in Montgomerie [126]). (Online version in colour.)

space. See appendix A for mathematical proofs of the equations and the role of each one of these assumptions:

(1) Small angles (less than or equal to 30°). Outside of this range, the signal due to iridescence is often very low and all that remains is the effect of the underlying pigments, which can be measured through traditional methods. For all thin films, and in some multilayers (depending on chemical composition), it is possible to consider angles up to 45°, as illustrated in the electronic supplementary material. This may help in producing more repeatable parameter estimates. For instance, a 45° angle can correspond to a viewer standing next to the viewed iridescent patch illuminated from above. Many previous studies have in this way mimicked the position of the bird relative to the sun in their measurements [66,87,98,105,114,118].
(2) The orientation of the layers within the multilayer structure is affected by Gaussian noise. Many developmental processes are controlled by a large array of independent factors of small effect each, causing subsequent errors to often be Gaussian (due to the central limit theorem). This assumption is also empirically supported by the results of Gur *et al.* [127], who looked at the orientation of guanine crystals in neon tetra fishes (*Paracheirodon innesi*) using wide-angle X-ray scattering. Fitting a Cauchy distribution (fatter tail distribution) instead of a Gaussian distribution yields similar values of parameter estimates. For simplicity, we here only present the results with Gaussian noise.
(3) Multilayers are ideal, i.e. the optical thickness (layer thickness times optical index) of each layer is constant: $n_1e_1 = n_2e_2$. This is a common assumption [36,54,67,97, 107,119,128–130] which is thought to be valid for most animal reflectors [131] because it produces the brightest and most saturated signals with a minimal number of layers (but see Schultz & Rankin [35] and Parker *et al.* [132] for beetles, Kinoshita *et al.* [133] for neon tetra).

This set of assumptions allows us to formally derive simple analytic expressions of brightness B, hue H and saturation S (figure 1) in the angle space (Φ_{inc}, Φ_{col}). All variables used in this study with their notations and their possible values are listed in table 2 and illustrated whenever possible in figure 2.

$$B(\Phi_{inc}, \Phi_{col}) = B_{max} \exp -\frac{((\Phi_{inc} - \Phi_{col})/2 - t)^2}{2\gamma_B^2}, \quad \text{(A 4 bis)}$$

$$H(\Phi_{inc}, \Phi_{col}) = H_{max} \cos\left(\gamma_H \frac{\Phi_{inc} + \Phi_{col}}{2}\right) \quad \text{(A 14 bis)}$$

and

$$S(\Phi_{inc}, \Phi_{col}) = S_{max}. \quad (2.1)$$

Hereafter, we focus on brightness B and hue H because saturation S is constant no matter the angle configuration. The brightness $B(\Phi_{inc}, \Phi_{col})$ in the angle space is entirely defined by three parameters: B_{max}, t and γ_B. The tilt t is the angle between the multilayer structure and the sample surface (as illustrated in figure 2). B_{max} is the maximum reflectance produced by the multilayer or thin-film structure, reached when the fibres are placed in a symmetrical configuration relative to the normal of the multilayer. γ_B is the parameter quantifying the disorder in the alignment of the multilayer structure. This disorder in the structure results in a reflected signal that is not purely specular but instead contains a diffuse component, meaning it can be seen at multiple angle configurations. For this reason, from a macroscopic point of view, γ_B is correlated with the angular dependency of brightness. Earlier studies used a binary classification of iridescent colours depending on the angle range at which the colour was visible ('diffuse/directional' in Osorio & Ham [110], 'wide-angle/flashing' in Huxley [55], 'limited view' of Vukusic *et al.* [134]). This classification is positively correlated with $1/\gamma_B$.

The hue $H(\Phi_{inc}, \Phi_{col})$ in the angle space is defined by two parameters: H_{max} which is the hue at coincident geometry (when using a bifurcated probe for example) and γ_H is the angular dependency of hue.

The variations of brightness and hue in the angle space, according to equations (A 4) and (A 14), respectively, are represented in figure 3.

2.3. Angle and notation conventions

In the rest of this study, we measure the incoming light ray angles (θ_i and Φ_{inc}) counter-clockwise and the outgoing light ray angles (θ_r and Φ_{col}) clockwise. For both incoming and outgoing angles, the origin is the normal to the structures (θ_i and θ_r) or the normal to the sample (Φ_{inc} and Φ_{col}). These conventions are represented in figure 2 where the direction of the arrows on angles represents the positive direction. The tilt t corresponds to the angle between the multilayer and the surface of the sample and is defined as $t = \Phi_{inc} - \theta_i = \theta_r - \Phi_{col}$ (see appendix A for more details about t). In other words, t is positive when the multilayer is tilted towards the illumination and negative otherwise (i.e. t is measured clockwise).

3. Methods

3.1. Study system: hummingbirds and butterflies

We used hummingbirds and butterflies (more precisely some *Morpho* and *Papilio* species) as study systems. Hummingbirds make an ideal example to test our framework for numerous reasons. First, they belong to a speciose family where all species are iridescent [135], which allows us to work on a large number of species that diverged fairly recently [136]. Upon visual examination, they display highly different types of iridescent colours, with either 'diffuse' (usually on dorsal patches) or 'directional' (usually on facial or

Table 2. List of parameters used in this study, with their domains of definition and their meanings.

symbol	range	meaning
θ_i	$[-\frac{\pi}{2}; \frac{\pi}{2}]$	incident light angle relative to the multilayer
θ_r	$[-\frac{\pi}{2}; \frac{\pi}{2}]$	reflected light angle relative to the multilayer
θ_1	$[0; \frac{\pi}{2}]$	angle between the incident ray and the interface between layers 1 and 2
θ_2	$[0; \frac{\pi}{2}]$	angle between the transmitted ray and the interface between layers 1 and 2
		angle between the incident ray and the interface between layers 2 and 1
m	$\mathbb{N}$	interference order/rank
B	$\mathbb{R}^+$	brightness at a given configuration
H	$[\lambda_{min}; \lambda_{max}]$	hue at a given angle configuration
S	$\mathbb{R}^+$	saturation at a given angle configuration
B_{max}	$\mathbb{R}^+$	maximal brightness value (achieved for specular position)
t	$[-\frac{\pi}{2}; \frac{\pi}{2}]$	angle between the multilayer surface and the sample surface (=tilt)
γ_B	$\mathbb{R}^+$	disorder of the layer alignment in the multilayer/angular dependency of brightness
H_{max}	$[\lambda_{min}; \lambda_{max}]$	maximal hue value (achieved at normal incidence geometry)
γ_H	$\mathbb{R}^+$	angular dependency of hue
n	$\mathbb{C}$	optical index of the material
e	$\mathbb{R}^+$	thickness of the layer(s)
Φ_{inc}	$[-\frac{\pi}{2}; \frac{\pi}{2}]$	angle between incidence fibre and sample surface (measured counterclockwise)
Φ_{col}	$[-\frac{\pi}{2}; \frac{\pi}{2}]$	angle between collection fibre and sample surface (measured clockwise)
const.	$\mathbb{R}$	used to denote a constant whose value is not important for the calculations

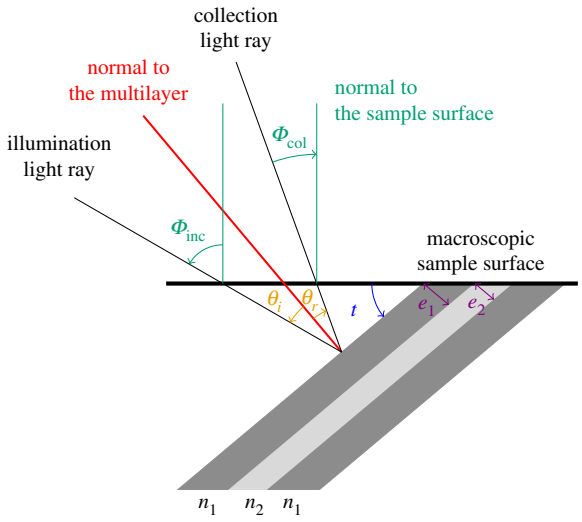

Figure 2. Schematic of a tilted multilayer (angle between the multilayer and the sample surface or tilt $t = 40^\circ$) and incoming and reflected light rays relative to the multilayer structure (with angles θ_i and θ_r, respectively) and relative to the sample surface (with angles Φ_{inc} and Φ_{col}, respectively). There is a relationship involving the tilt t between angles relative to the multilayer structure (θ_i and θ_r) and angles relative to the sample surface (Φ_{inc} and Φ_{col}): $\theta_i = \Phi_{inc} - t$ and $\theta_r = \Phi_{col} + t$. The positive direction for each angle is figured by an arrowhead. The multilayer is composed of an alternance of two layers characterized by the optical indices n_1 and n_2 and their thicknesses e_1 and e_2. A schematic at a different scale, focusing on the goniometer, is available in the electronic supplementary material. (Online version in colour.)

ventral patches) iridescence (*sensu* Osorio & Ham [110]). In addition, many species have highly tilted multilayers, providing a good test case to estimate the tilt t [110,114]. Finally, most species are available in large numbers in museum collections. We obtained the authorization from the Muséum National d'Histoire Naturelle to carefully cut feathers using surgical scissors. We selected one male from 36 species, evenly distributed across the phylogeny, from which we took feathers on two patches, one diffuse and one directional (*sensu* Osorio & Ham [110]).

Because the exclusive use of hummingbirds as a test taxon for a new method has been criticized in previous studies [86], we also test our method on a very different group: butterflies. Butterflies are phylogenetically distant from birds and have different structures producing iridescence. For these reasons, the fact our method works in both taxa is a compelling argument for its universality. We used 17 butterfly species known to have multilayer structures [101,137]. The full list of species we used for our measurements is available in the electronic supplementary material, for both hummingbirds and butterflies.

The method presented is also valid for whole specimens (whole birds instead of plucked feathers, for example). We nonetheless opted for the use of single feathers to maximize repeatability. Indeed, the precision of the goniometer measurements relies on the fact that the sample is precisely located at the centre of rotation of both fibres, which is more difficult to ensure for whole specimens.

3.2. Reflectance measurements

We measured reflectance at various angles using a purpose-built goniometer, following the recommendations of Meadows *et al.* [114]. The light emitted by a xenon lamp (300 W) over the 300–700 nm range of wavelengths to which birds are sensitive [138] was brought to the sample through an illuminating UV–visible optical fibre collimated to get a 1 mm light spot at normal illumination. Light reflected by the sample was then collected by a second identical collimated optical fibre and conducted toward an Oceanoptics USB4000 spectrophotometer. This set-up allows for a precise independent rotation of the illumination and the collection fibres, necessary for the measurements of iridescent colours.

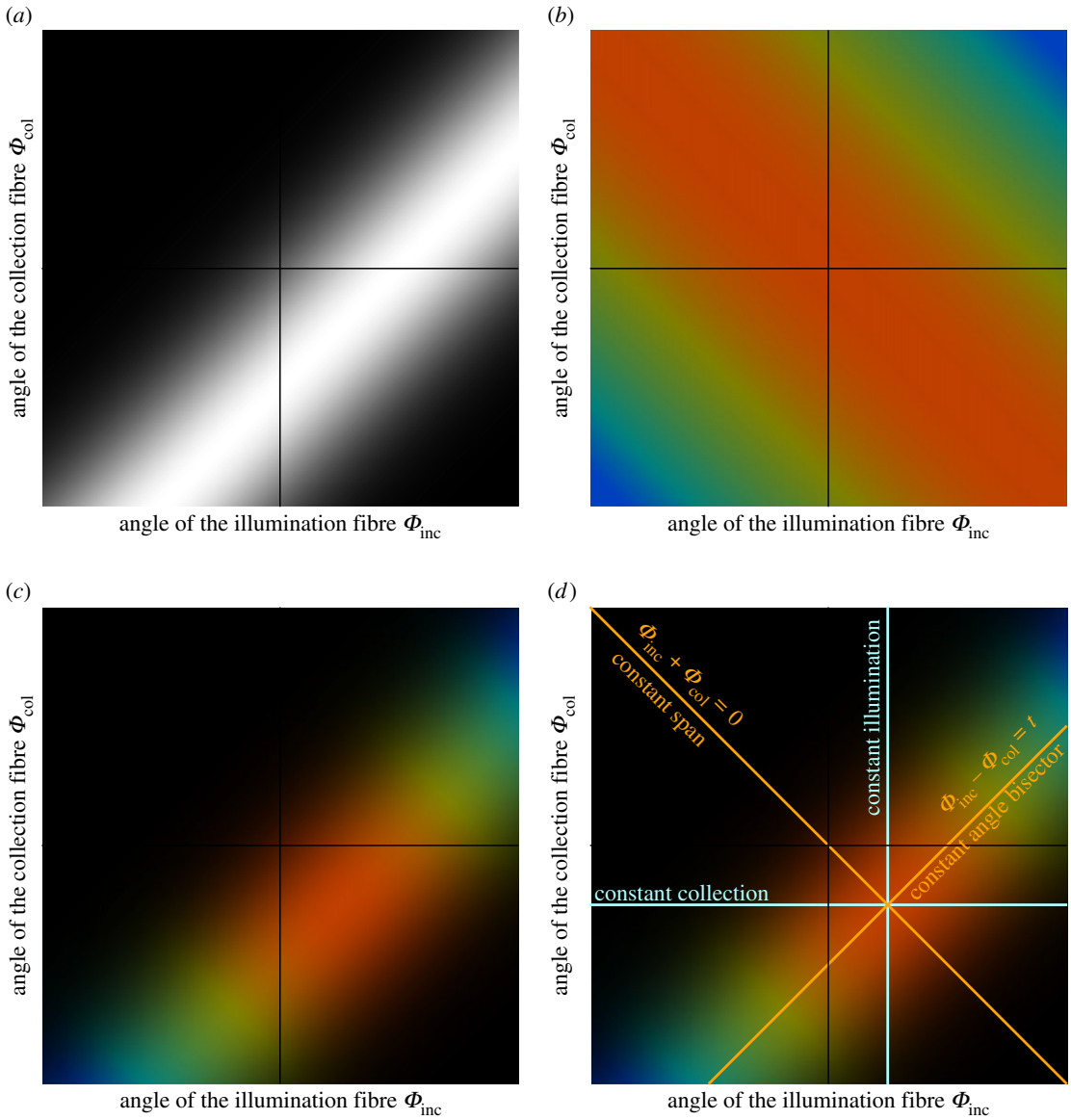

Figure 3. Colour variables (*a*) brightness, (*b*) hue, (*c*) and (*d*) hue and brightness of an iridescent multilayer (with tilt $t \neq 0$) in the angle space relative to the sample surface (Φ_{inc}, Φ_{col}). The colour lines in (*d*) indicate alternative bases: the angle space relative to the multilayer structure (θ_i, θ_r) in blue and ($\Phi_{inc} + \Phi_{col} = 0$, $\Phi_{inc} - \Phi_{col} = t$) in orange and illustrates the terms 'constant illumination', 'constant collection', 'constant angle bisector' and 'constant span' used in table 1 and throughout this article.

Our previous mathematical exploration (detailed in appendix A.2) revealed that hue is constant along the $\Phi_{inc} + \Phi_{col} = \text{const.}$ line (constant span) and brightness along the $\Phi_{inc} - \Phi_{col} = \text{const.}$ line (constant angle bisector), as illustrated in figure 3. We thus only need to take measurements in two orthogonal directions: in the direction $\Phi_{inc} - \Phi_{col} = \text{const.}$ to quantify hue variation and in the direction $\Phi_{inc} + \Phi_{col} = \text{const.}$ to quantify brightness variations. This will allow us to infer all parameters controlling hue and brightness, and therefore to potentially compute all values of hue and brightness in the entire angle space (Φ_{inc}, Φ_{col}).

The shape and size of the light spot on the sample depend on the position of the illuminating fibre relative to the sample. As the angle of illumination θ_i increases, the light spot becomes more and more elongated, according to a θ_i cosine function. This means the amount of light received by the spectrometer decreases when θ_i increases, independently of sample characteristics. This can also be empirically observed by taking measurements of the white reference (which is a Lambertian surface, i.e. reflectance does not depend on the angle) at different angles. To control for this, we took white reference measurements at several angle configurations (detailed in the protocol below). The white standard for this study was an Avantes reference tile WS-2. Because this is a diffuse (Lambertian) white reference and because some iridescent colours are very directional (i.e. all reflected light is focused in a single direction), it is expected to sometimes get values of brightness that can be over 100%.

The detailed protocol we used for our measurements is similar to Waldron *et al.* [118] and inspired from Osorio & Ham [110] and Meadows *et al.* [114]. A detailed walk-through of the measurement protocol is presented in box 1, and a worked example is available in the electronic supplementary material.

We repeated each measurement twice, on different days, by two different experimenters for hummingbirds and butterflies. We performed statistical analyses after the completion of the measurement session to prevent experimenter bias.

3.3. Statistical analyses

As explained in the previous section, the angle configuration changes the shape of the light spot and thus the total possible amount of light collected by the collection fibre. To address this issue, we first pre-processed spectra to normalize count data using the appropriate reference white spectrum (script available in the electronic supplementary material). Resulting `csv` files were then imported in `pavo` R package [139]. Hue values were discarded (i.e. converted to `NA`) when brightness was lower than 8.5% because hue is not defined for black colours.

Box 1. Measurement protocol.

(1) Move one of the two fibres of the goniometer to find the position where you get a signal of maximal intensity. This position depends on the tilt t of the multilayer and is therefore different for every sample. Once this is done, this means the angle bisector of the two fibres is close to the normal to the multilayer structure (red line in figure 2).
(2) While keeping the same angle bisector, take measurements at different angular spans (orange line $\Phi_{inc} - \Phi_{col} = t$ in figure 3*d*). These measurements will be used to estimate hue parameters. To have a sample size large enough for reliable estimation and to stay at small angles, we recommend measurements at $(\Phi_{inc}, \Phi_{col}) \in \{(t + 5^\circ, t + 5^\circ), (t + 10^\circ, t + 10^\circ), (t + 15^\circ, t + 15^\circ), (t + 20^\circ, t + 20^\circ), (t + 25^\circ, t + 25^\circ)\}$.
(3) Take measurements while keeping the angular span between the two fibres constant (e.g. $\Phi_{col} - \Phi_{inc} = 20^\circ$) and moving the angle bisector (if you cannot do this, because for example, one of your fibres is not mobile, see appendix B.2). This will be used to estimate parameters related to brightness. We recommend three measurements on each side of the supposed normal to the multilayer structure (seven measurements in total) and a span of 20°: $(\Phi_{inc}, \Phi_{col}) \in \{(t - 5^\circ, t + 25^\circ), (t^\circ, t + 20^\circ), (t + 5^\circ, t + 15^\circ), (t + 10^\circ, t + 10^\circ), (t + 15^\circ, t + 5^\circ), (t + 20^\circ, t + 0^\circ), (t + 25^\circ, t - 5^\circ)\}$. Depending on how directional your sample is, it may be needed to increase the resolution of the measurement grid and only move the angle bisector of 2.5° or 5° at each step.
(4) Take white reference measurements with the same angular spans as before but using the normal to the goniometer as angle bisector (same measurements as in 2 but with $t = 0^\circ$). If you have followed our advice for measurements, you should now take white measurements at $(\Phi_{inc}, \Phi_{col}) \in \{(5^\circ, 5^\circ), (10^\circ, 10^\circ), (15^\circ, 15^\circ), (20^\circ, 20^\circ), (25^\circ, 25^\circ), (30^\circ, 30^\circ)\}$.
(5) Take white reference measurements with a constant span but various angle bisectors (same measurements as in 3 but with $t = 0^\circ$). If you have followed our advice of three measurements on each side to the supposed normal to the multilayer structure and a span of 20°, you should now take white measurement at $(\Phi_{inc}, \Phi_{col}) \in \{(-5^\circ, 25^\circ), (0^\circ, 20^\circ), (5^\circ, 15^\circ), (10^\circ, 10^\circ), (15^\circ, 5^\circ), (20^\circ, 0^\circ), (25, -5^\circ)\}$.

Iridescence parameters can be estimated using various methods, including least-squares optimization and Bayesian non-linear regression. We used a least-squares optimization as it is more common in biological sciences. We tested the Bayesian approach as well but it returned similar results and it is therefore not presented here.

We used two indices to estimate the variability of the parameters resulting from our method: (i) relative standard deviation (RSD, also called coefficient of variation or CV) as the standard deviation divided by the absolute value of the mean. (Absolute) standard deviation (SD) is a common measure of the noise in a dataset. RSD is a way to quantify the signal-to-noise ratio. Because it is normalized by the mean value of the parameter, it is dimensionless and can be compared between parameters. It represents the precision of the experimental and statistical framework and does not depend on the sample population. (ii) Repeatability as the intra-class coefficient (ICC) computed with the `rptR` package [140]. ICC assesses whether the method allows one to discriminate individual samples among the population by comparing intra- and inter-sample standard deviation. ICC is therefore highly dependent on the sample population and on the biological question.

RSD and ICC complement each other. A very precise method can still lead to non-repeatable measurements if there is no variability in the population. Conversely, a coarse method can work well enough to discriminate between samples and be repeatable if the variability between samples is high.

4. Results and discussion

Spectra from measurement along the 'constant span' ($\Phi_{inc} + \Phi_{col} = 20^\circ$) and 'constant angle bisector' ($\Phi_{inc} - \Phi_{col} = \text{const.}$) lines after correction by the appropriate white reference are displayed in figure 4 for the iridescent blue of the breast of the hummingbird *Heliomaster furcifer*. We also show values of hue H and brightness B along these two measurement lines as well as the result from parameter estimation.

4.1. Relative error and repeatability

Variability and repeatability results are summarized in table 3. We find low values of RSD for hue-related variables for both hummingbirds and butterflies, indicating that our framework provides precise estimations of parameters. For brightness-related parameters, RSD is higher, as is usually the case, even for non-iridescent colours [141–143]. Despite relatively high RSD, all values for brightness remain repeatable, expected tilt t for butterflies because of a low inter-species variability, as demonstrated by the low value of SD.

4.2. Correlation between parameters

4.2.1. Correlation between B_{max} and γ_B

Madsen *et al.* [105] noticed a negative relationship between brightness angular dependency and maximum brightness. From an evolutionary point of view, this means there is a trade-off between the signal brightness at a given angle and the range of angle at which it is not black (i.e. directionality *sensu* Osorio & Ham [110]).

This correlation can also be proved theoretically. Indeed, the total energy of light that is reflected by the sample cannot exceed the received light energy. In other words, if absorption is similar across samples, the total brightness reflected in all directions is constant across samples:

$$\iint B(\Phi_{inc}, \Phi_{col})\, d\Phi_{inc}\, d\Phi_{col} = \text{const.} \tag{4.1}$$

The value of this double integral is known ($B(\Phi_{inc}, \Phi_{col})$ is a bivariate Gaussian function) and when we compute it, we find

$$B_{max}\sqrt{2\pi\gamma_B^2} = \text{const.} \tag{4.2}$$

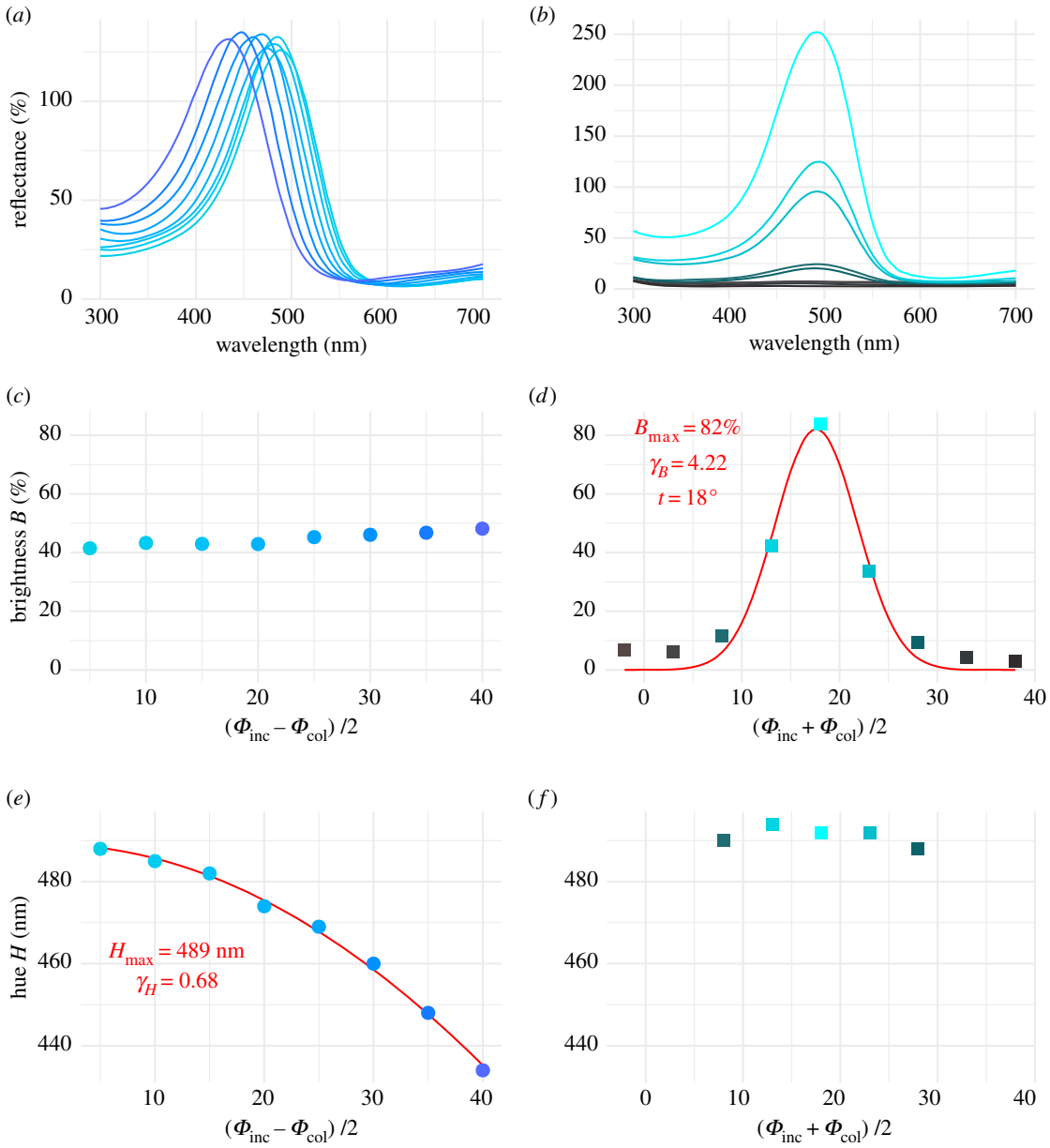

Figure 4. Spectra (*a*,*b*) and corresponding values of brightness (*c*,*d*) and hue (*e*,*f*) at different angle configurations for the breast patch of the hummingbird *Heliomaster furcifer* along the $\Phi_{inc} - \Phi_{col} = \text{const.}$ (*a*,*c*,*e*; data points with round shape) and $\Phi_{inc} + \Phi_{col} = \text{const.}$ (*b*,*d*,*f*; data points with square shape) lines. Colours correspond to the conversion of the spectra in human vision using the CIE10 visual system. As expected, brightness is constant when $\Phi_{inc} - \Phi_{col} = \text{const.}$ and has a Gaussian shape when $\Phi_{inc} + \Phi_{col} = \text{const.}$ Conversely, hue has a cosine shape when $\Phi_{inc} - \Phi_{col} = \text{const.}$ and is constant when $\Phi_{inc} + \Phi_{col} = \text{const.}$ The red lines correspond to the fit of the functions after parameter estimation, with the values of the parameters. The R script to produce this figure is available in electronic supplementary material.

Table 3. Repeatability (ICC with likelihood ratio and permutation *p*-values) and standard deviations (SD and RSD) of iridescence parameters for hummingbirds and butterflies.

taxon	variable	param.	mean	SD	RSD (%)	ICC	*p* (likel.)	*p* (perm.)
hummingbirds	brightness	B_{max}	36.60	47.54	14.79	0.947	<0.0001	0.001
		t	14.61	18.21	7.428	0.968	<0.0001	0.001
		γ_B	13.67	7.85	11.19	0.875	0.0009	0.002
	hue	H_{max}	556.80	65.66	0.3004	0.997	<0.0001	0.001
		γ_H	0.64	0.18	2.281	0.689	0.028	0.098
butterflies	brightness	B_{max}	148.80	99.78	6.91	0.936	<0.0001	0.001
		t	2.94	4.83	32.96	0.268	0.18	0.098
		γ_B	5.35	5.12	4.76	0.769	<0.0001	0.004
	hue	H_{max}	492.69	27.87	0.2484	0.993	<0.0001	0.001
		γ_H	0.73	0.14	2.993	0.853	<0.0001	0.001

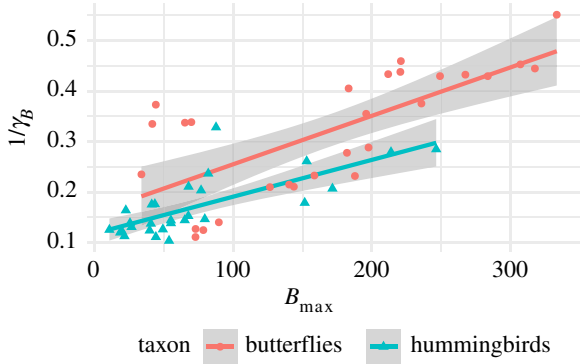

Figure 5. Correlation between B_{max} and directionality $1/\gamma_B$. The dots are the data points. The lines show the result of the generalized linear model. (Online version in colour.)

and

$$B_{max} \propto \frac{1}{\gamma_B}. \tag{4.3}$$

We indeed find a positive correlation between B_{max} and $1/\gamma_B$ in the empirical data ($F = 147.0742$, d.f. $= 1$, $p < 0.0001$), illustrated in figure 5. We also notice an effect of the taxon (butterflies or hummingbirds) on the slope of the correlation ($F_1 = 8.3198$, $p = 0.0057$). Because the link between B_{max} and $1/\gamma_B$ was proven when ignoring absorption (equation (4.3)), this may suggest that absorption is higher in hummingbirds than in butterflies.

4.2.2. Correlation between angular dependency for hue γ_H and other parameters.

Osorio & Ham [110] found that γ_H and γ_B are negatively correlated among 15 bird species from different families. We do not find support for such correlation for either the hummingbirds or the butterflies ($F_1 = 3.1994$, $p = 0.074$; figure in electronic supplementary material). Additionally, as discussed later in appendix B.3.2, many studies use variables that are correlated to H_{max} to quantify hue angular dependence. On the contrary, we find that the parameters used in our method, H_{max} and γ_H, are not correlated ($F_1 = 0.5167$, $p = 0.47$; figure in electronic supplementary material).

5. Conclusion

Using both a theoretical and an experimental approach we find that hue and brightness can be easily characterized for all angle configurations using a set of five parameters (H_{max} and γ_H for hue; B_{max}, t and γ_B for brightness). Additionally, we show that a relatively small number of measurements is sufficient to reliably estimate these parameter values. This is made possible by the fact that hue is constant when the angular span between the two fibres remains constant ($\Phi_{inc} - \Phi_{col} = \text{const.}$), and that brightness is constant for small angles as long as the angle bisector remains in the same position ($\Phi_{inc} + \Phi_{col} = \text{const.}$) (as illustrated in figures 3 and 4). These properties have been previously noticed empirically for hue H_1 by Osorio & Ham [110] on 15 bird species sampled from different families and Meadows *et al.* [114] on *Calypte anna*. Without being formalized, it had been illustrated for brightness in Eliason & Shawkey [104] and Stavenga *et al.* [77] for B_3 as well as Stavenga *et al.* [78] for B_1.

Our contribution unlocks new perspectives for studies on iridescent colours, such as the evolution of complex visual signals leveraging angular dependency properties of iridescent colours.

The proofs for the equation in this article are based on the multilayer theory. However, it is possible that parts of it may work for iridescence from diffraction gratings. Future studies should aim at integrating iridescence from diffraction into our framework. This would allow for a standard set of variables to describe iridescence, no matter its physical origin. Further investigation is also required to assess whether it is possible to relax some of the assumptions made in the paper under certain conditions.

Data accessibility. Data used in this study as well as scripts to apply the described method are available in the electronic supplementary material.

Authors' contributions. H.G. conducted the study (model construction, data analysis) and wrote the first version of this manuscript. H.G. performed measurements on hummingbirds and D.G. on butterflies. W.D.d.M. designed and built the goniometer. C.A., D.G., M.E. and S.B. contributed to the design of the goniometer. C.A., D.G. and W.D.d.M. helped with measurement protocol. D.G. and M.E. participated in the discussion for biological significance and pitfalls. All authors contributed to the final version of this article.

Competing interests. The authors declare no competing interests.

Funding. No funding has been received for this article.

Acknowledgements. We are grateful to C. Doutrelant and two anonymous reviewers for their valuable comments on the manuscript. We would also like to thank the Muséum National d'Histoire Naturelle and in particular J. Fuchs, P. Boussès and A. Previato for letting us sample feathers from museum hummingbird specimens, as well as V. Debat for lending us *Morpho* specimens to explore *Morpho* iridescence. Finally, we thank the Living Light conference organizers for putting together this special issue on structural colours in living organisms.

Appendix A. Mathematical proof of the equations

A.1. Brightness B in the angle space (Φ_{inc}, Φ_{col})

For a perfectly regular multilayer, all the reflected signal is focused in the specular direction, at an angle θ_r equal to the incident angle θ_i. The brightness B is proportional to the reflected signal intensity, meaning

$$B(\theta_i, \theta_r) = \begin{cases} B(\theta_i) & \text{if } \theta_i = \theta_r \\ 0 & \text{if } \theta_i \neq \theta_r, \end{cases} \tag{A 1}$$

where $B(\theta_i)$ is defined by the Fresnel factor in the case of a thin-film structure (equation and R code to compute the Fresnel factor available in the electronic supplementary material). However, because we are dealing with small angles (assumption 1), we can approximate $B(\theta_i)$ to a constant B_{max} (as illustrated in the electronic supplementary material):

$$B(\theta_i, \theta_r) \approx \begin{cases} B_{max} & \text{if } \theta_i = \theta_r \\ 0 & \text{if } \theta_i \neq \theta_r. \end{cases} \tag{A 2}$$

But because biological structures are not entirely flat, and because the different layers of the multilayer structure are not perfectly aligned, there is also some amount of light reflected outside of the specular reflection (often referred as diffuse reflection). We thus assume a Gaussian decay of the brightness B around the specular position $\theta_i = \theta_r$ (assumption 2), controlled

by a parameter γ_B related to the disorder of the multilayer:

$$B(\theta_i, \theta_r) \approx B_{\max} \exp -\frac{((\theta_i - \theta_r)/2)^2}{2\gamma_B^2}. \quad \text{(A 3)}$$

In the case of a perfectly regular multilayer with no disorder, we have $\gamma_B = 0$ and we find equation (A 2). Conversely, if $\gamma_B = +\infty$, the brightness value is the same for all angle configurations, which means we are dealing with a Lambertian surface.

Additionally, the multilayer structure is not always parallel to the sample surface. It is the case, for example, for hummingbirds included in this study, as well as for *Morpho* butterflies in Berthier *et al.* [67], for the rainbow stag beetle, *Phalacrognathus muelleri*, structures described by Edo *et al.* [109], six pierid butterflies in Pirih *et al.* [102], 10 species of butterflies in Wickham *et al.* [80], and for six species of *Heliconius* butterflies in Parnell *et al.* [96]. So the illuminating angle Φ_{inc} and the collection Φ_{col} at the macroscopic scale do not necessarily match θ_i and θ_r (as illustrated in figure 2). If we denote t the angle between the multilayer surface and the macroscopic sample surface (called *tilt* hereafter, as in Madsen *et al.* [105] and Osorio & Ham [110]), we get

$$B(\Phi_{\text{inc}}, \Phi_{\text{col}}) \approx B_{\max} \exp -\frac{((\Phi_{\text{inc}} - \Phi_{\text{col}})/2 - t)^2}{2\gamma_B^2}. \quad \text{(A 4)}$$

Using equation (A 4), we only have three parameters ($B_{\max}$, t and γ_B) to estimate to be able to reconstruct all values of brightness B in the angle space defined by (Φ_{inc}, Φ_{col}). The resulting brightness in this space in plotted in figure 3.

A.2. Hue H in the angle space (Φ_{inc}, Φ_{col})

We defined the hue H as the wavelength for which reflectance is maximal. In the context of interferences, it is therefore the wavelength for which reflected light interferes constructively. For a regular multilayer, this happens when

$$mH(\theta_1, \theta_2) = 2(n_1 e_1 \cos\theta_1 + n_2 e_2 \cos\theta_2), \quad \text{(A 5)}$$

where m is an integer (interference order), θ_1 is the angle between the incident light ray and the multilayer structure at the interface between layer 1 and 2, θ_2 is the angle between the transmitted ray after going through the first interface between layers 1 and 2 and the multilayer structure, n_1 and n_2 are the optical indices of the layers, and e_1 and e_2 the thicknesses of the layers. The products n_1e_1 and n_2e_2 are often called optical thicknesses of the layers 1 and 2 (respectively).

The relationship between θ_1 and θ_2 is given by Snell's Law:

$$n_1 \sin\theta_1 = n_2 \sin\theta_2. \quad \text{(A 6)}$$

Because $\theta_1 \in [0; \pi/2]$, hue H increases when angle θ_1 decreases according to equation (A 5). This means a maximum value for hue $H_{\max}$ is achieved when $\theta_1 = 0$ (in this case $\theta_2 = 0$ as well because of Snell's Law; equation (A 6)):

$$mH_{\max} = 2(n_1 e_1 + n_2 e_2). \quad \text{(A 7)}$$

We can replace n_1e_1 and n_2e_2 in equation (A 5) using equation (A 7):

$$mH(\theta_1, \theta_2) = mH_{\max}(\cos\theta_1 + \cos\theta_2) - 2(n_1 e_1 \cos\theta_2 + n_2 e_2 \cos\theta_1). \quad \text{(A 8)}$$

By adding equation (A 8) and equation (A 5), we obtain

$$2mH(\theta_1, \theta_2) = mH_{\max}(\cos\theta_1 + \cos\theta_2) + 2(\cos\theta_1 - \cos\theta_2)(n_1 e_1 - n_2 e_2). \quad \text{(A 9)}$$

We consider here the case of an ideal multilayer, meaning that $n_1e_1 = n_2e_2$ (assumption 3). This allows us to simplify equation (A 9) into

$$H(\theta_1, \theta_2) = H_{\max} \frac{\cos\theta_1 + \cos\theta_2}{2}. \quad \text{(A 10)}$$

Because we are working with small angles (assumption 1), Snell's Law (equation (A 6)) can be approximated by

$$\theta_2 \approx \frac{n_1}{n_2}\theta_1 \quad \text{(A 11)}$$

and

$$H(\theta_1, \theta_2) \approx H_{\max} \frac{\cos\theta_1 + \cos(n_1/n_2)\theta_1}{2}. \quad \text{(A 12)}$$

For small angles (assumption 1), this sum of cosine functions can be approximated by a single cosine function with twice the amplitude (numerical proof in the electronic supplementary material):

$$H(\theta_1, \theta_2) \approx H_{\max} \cos\gamma_H\theta_1, \quad \text{(A 13)}$$

where $\gamma_H \approx \sqrt{(1 + (n_1/n_2)^2)/2}$ (after identification of the coefficients of the second-order Taylor series expansions in equations (A 12) and (A 13)).

This reasoning is valid for ideal thin-film structures and multilayers and tells what happens at the specular position. But as explained in the previous section, biological structures are noisy and there is signal outside the specular position. As previously, if there is signal, this means that there is a multilayer for which the position of the fibres is specular. And in this case, we can apply equation (A 13) as well:

$$H(\Phi_{\text{inc}}, \Phi_{\text{col}}) = H_{\max} \cos\left(\gamma_H \frac{\Phi_{\text{inc}} + \Phi_{\text{col}}}{2}\right). \quad \text{(A 14)}$$

We only need two parameters ($H_{\max}$ and γ_H) to plot all hue values in the angle space (Φ_{inc}, Φ_{col}) as in figure 3. In the case of non-iridescent colours, we have $\gamma_H = 0$.

A.3. Saturation S in the angle space (Φ_{inc}, Φ_{col})

A.3.1. Along the 'constant span' direction ($\Phi_{\text{inc}} + \Phi_{\text{col}} =$ const.)

We know that along the $\Phi_{\text{inc}} + \Phi_{\text{col}} =$ const. direction (constant span), hue is constant (as shown in equation (A 14) and figure 3*b*). Using a similar reasoning as in appendix A.1, we find that the reflectance R for a wavelength λ at a given angle configuration (Φ_{inc}, Φ_{col}) is given by

$$R(\Phi_{\text{inc}}, \Phi_{\text{col}}, \lambda) = R_{\text{bisector}}(\lambda) \exp -\frac{((\Phi_{\text{inc}} - \Phi_{\text{col}})/2 - t)^2}{2\gamma_B^2}. \quad \text{(A 15)}$$

This means that reflectance spectra at all angle configurations along the 'constant span' axis ($\Phi_{\text{inc}} + \Phi_{\text{col}} =$ const.) can be derived by scaling of the spectrum at another angle configuration.

The saturation $S(\Phi_{\text{inc}}, \Phi_{\text{col}})$ is defined as the full width at half maximum of the reflectance spectrum $R(\Phi_{\text{inc}}, \Phi_{\text{col}}, \lambda)$. Let us call R the reflectance spectrum at a given angle configuration

$(\Phi_{inc}^{pos1}, \Phi_{col}^{pos1})$. Then the saturation S at this configuration is

$$\left.\begin{aligned} &S = \lambda_1 - \lambda_2, \\ &R(\lambda_1) = R(\lambda_2) = \frac{R_{max}}{2} \\ \text{and}\quad &\lambda_1 > \lambda_2. \end{aligned}\right\} \tag{A 16}$$

If the reflectance spectrum R' at $(\Phi_{inc}^{pos2}, \Phi_{col}^{pos2})$ is equal to R scaled by a factor s, then the saturation S' is

$$\left.\begin{aligned} &S' = \lambda_1' - \lambda_2', \\ &R'(\lambda_1') = R'(\lambda_2') = \frac{R'_{max}}{2} \\ \text{and}\quad &\lambda_1' > \lambda_2', \end{aligned}\right\} \tag{A 17}$$

where

$$\left.\begin{aligned} &R'(\lambda_1') = \frac{R(\lambda_1')}{s}, \\ &R'(\lambda_2') = \frac{R(\lambda_2')}{s} \\ \text{and}\quad &R'_{max} = \frac{R_{max}}{s}. \end{aligned}\right\} \tag{A 18}$$

From this, we find that

$$\frac{R(\lambda_2')}{s} = \frac{R(\lambda_1')}{s} = \frac{R_{max}}{2s} \tag{A 19}$$

and

$$R(\lambda_2') = R(\lambda_1') = \frac{R_{max}}{2}. \tag{A 20}$$

This means that $\lambda_1' = \lambda_1$ and $\lambda_2' = \lambda_2$. In other words, the full width at half maximum is stable by scaling, which results in the saturation S remaining constant along the $\Phi_{inc} + \Phi_{col} =$ const. axis (constant span).

A.3.2. Along the 'constant angle bisector' direction ($\Phi_{inc} - \Phi_{col} =$ const.)

Additionally, along the $\Phi_{inc} - \Phi_{col} =$ const. axis (constant angle bisector), brightness is constant and only hue changes. This means spectra are translations of one another. The full width at half maximum is also stable by translation so the saturation S remains constant along $\Phi_{inc} - \Phi_{col} =$ const. axis (constant angle bisector).

A.3.3. In the general case

All points in the (Φ_{inc}, Φ_{col}) space can be reached by a combination of moves along the orthogonal 'constant span' ($\Phi_{inc} + \Phi_{col} =$ const.) and 'constant angle bisector' ($\Phi_{inc} - \Phi_{col} =$ const.) axes. We just showed the saturation S is constant along these two axes so it is actually constant in the whole (Φ_{inc}, Φ_{col}) space.

Appendix B. Comparison with other methods

B.1. Measurements at fixed angle configuration

The angle t between the multilayer structure and the normal to the surface of the feather (tilt) is highly variable between species of the same family (SD = 19.36° in hummingbirds, as reported in table 3). This is in agreement with Osorio & Ham [110] who found tilt values t ranging from −20° to 40°. Even if the angle configuration (Φ_{inc}, Φ_{col}) is constant at the macroscopic scale, the configuration relative to the multilayer structure (θ_i, θ_r) may not be constant because of the variation in the tilt t between samples. This means measurements at fixed geometry cannot be compared between samples. For this reason, we warn against measurements of iridescent colours at a fixed angle, even when angular dependency is not studied.

B.2. Parameter estimation using constant illumination

Some goniometers only allow for the rotation of the collection fibre while the illumination fibre stays at a fixed position. Measurements realized with a such protocol can still be used with our method but this leads to a loss of statistical power.

If illumination is provided at a fixed angle $\Phi_{inc} = \alpha$:

$$\begin{aligned} B(\Phi_{col}) &= B_{max} \exp - \frac{((\alpha - \Phi_{col})/2 - t)^2}{2\gamma_B^2} \\ &= B_{max} \exp - \frac{(\Phi_{col} + 2t - \alpha)^2}{8\gamma_B^2}. \end{aligned} \tag{B 1}$$

So, $B(\Phi_{col})$ is still a normal function of Φ_{col} with the same maximum value B_{max} but with parameters $t^* = 2t - \alpha$ and $\gamma_B{}^* = 2\gamma_B$ for mean and standard deviation, respectively.

Because the estimation of the parameters of a normal function through a regression is more reliable when the standard deviation is low, using anything else than a fixed normal as measurement line, such as a fixed illumination, to study brightness parameters will result in less accurate values.

Additionally, depending on the exact value of α, it may not be possible to have a fibre configuration where $(\alpha + \Phi_{col})/2 = t$ but the span between the fibres is still less than 90° (small angles assumption). In this case, data points never reach the maximum B_{max}, which makes parameter estimation very unreliable.

Finally, the new value of the mean t^* does not have a direct biological and physical interpretation, as opposed to t which is the tilt of the multilayer of thin-film structure.

For hue, if illumination is at fixed angle α

$$H(\Phi_{col}) = H_{max} \cos\left(\gamma_H \frac{\alpha}{2} + \frac{\gamma_H}{2} \Phi_{col}\right). \tag{B 2}$$

The equation for hue at fixed illumination has a shape different from its general form depending on the span between the fibres, $(\Phi_{inc} + \Phi_{col})/2$. There is a constant term in the cosine function and the new term for hue angular dependency is $\gamma_H{}^* = \gamma_H/2$. As we explain in the next section, the estimation of the parameters is more reliable for high values of γ_H. For this reason, the parameter estimation at fixed illumination may not be as precise as along the $\Phi_{inc} + \Phi_{col} =$ const. line.

B.3. Link with other variables of angular dependency for hue

B.3.1. Linear regression

Linear regression instead of cosine regression to estimate H_{max} and γ_H is common [63,75,110,121]. Because the curvature of the cosine function in equation (A 14), defining hue depending on the angular span, is often small, we obtain congruent results using either cosine or linear regression. However, this creates a systematic bias where H_{max} is more overestimated for samples with larger angle dependency γ_H. Indeed, a linear regression

overestimates more the intercept value as the curvature of the function increases.

B.3.2. Difference between two angle configurations with the same angle bisector

The difference in hue between two angle configurations is sometimes used as a proxy for iridescence [71]. However, it is problematic because it leads to a very high correlation between hue and iridescence, as reported in Dakin & Montgomerie [66] ($R^2 > 0.95$).

We can prove mathematically this linear correlation. Let us focus on the difference between hue H_{pos1} at a given angle configuration (Φ^1_{inc}, Φ^1_{col}) and hue H_{max} at coincident geometry (i.e. $\Phi_{inc} + \Phi_{col} = \theta_i + \theta_r = 0$). It follows from equation (A 14) that defines the hue at any angle configuration that:

$$H_{pos1} - H_{max} = H_{max}\left[\cos\left(\gamma_H \frac{\Phi^1_{inc} + \Phi^1_{col}}{2}\right) - 1\right]. \quad \text{(B 3)}$$

From this equation, we see that if γ_H is constant or displays low variability between samples, $H_{pos1} - H_{max}$ is proportional to H_{max}:

$$H_{pos1} - H_{max} \propto H_{max}. \quad \text{(B 4)}$$

We can apply the same reasoning and prove the difference $H_{pos2} - H_{max}$ between hue H_{pos2} at (Φ^2_{inc}, Φ^2_{col}) and H_{max} is proportional to H_{max}:

$$H_{pos2} - H_{max} \propto H_{max}. \quad \text{(B 5)}$$

Thus (doing equations (B 4) and (B 5)), the difference in hue between any two angle configurations (Φ^1_{inc}, Φ^1_{col}) and (Φ^2_{inc}, Φ^2_{col}) is proportional to H_{max}:

$$H_{pos1} - H_{pos2} \propto H_{max}. \quad \text{(B 6)}$$

This correlation between the two variables characterizing hue in the angle space can lead to errors in subsequent statistical inferences. On the opposite and as reported in §4.2.2, the parameters proposed in this study (H_{max} and γ_H) do not have the same issue.

B.4. Link with other variables of angular dependency for brightness

We are providing the following comparison with variables that have been previously used in the literature to describe brightness angular dependency. This means that values from previous studies using these variables can still be used in a meta-analysis or a discussion using our new variables B_{max}, t and γ_B. We however explain why they are less precise, less versatile and/or more time consuming than those measured under our unified framework.

B.4.1. Full width at half maximum and angular breadth

We have shown brightness is a Gaussian function of standard deviation γ_B along the line of 'constant span' ($\Phi_{inc} + \Phi_{col} =$ const. direction). Many studies previously characterized angular dependency in this direction using the full width at half maximum (hereafter FWHM) [80,102,107,110,113]. For a Gaussian function, there is an easy link between standard deviation and FWHM:

$$\begin{aligned} \text{FWHM} &= 2\gamma^*_B\sqrt{2\ln 2} \\ &= 4\gamma_B\sqrt{2\ln 2} \\ &\approx 4.71\gamma_B. \end{aligned} \quad \text{(B 7)}$$

Similarly, some studies use what they call *angular breadth* [85,86,88–92,112], which they define as the range of angle where brightness is higher than 3% of its maximum (threshold at 10% for [112]):

$$\begin{aligned} \text{ang. breadth} &= 2\gamma^*_B\sqrt{4\ln 10 - 2\ln 3} \\ &= 4\gamma_B\sqrt{4\ln 10 - 2\ln 3} \\ &\approx 10.59\gamma_B. \end{aligned} \quad \text{(B 8)}$$

We see that these variables are proportional to γ_B in theory. However because they are computed from raw data, without any pre-processing or curve fitting, they are more sensitive to noise.

B.4.2. Hunter's specular gloss and integrating sphere

Multiple studies [75,144,145] use Hunter's gloss [146], defined by the ratio of specular to diffuse reflectance. This method is convenient because it can easily be achieved using an integrating sphere to capture the needed spectra in two measurements only (one at specular position without the sphere and one with the sphere to capture diffuse and specular reflectance).

This is equivalent to keeping the illumination at a fixed angle and measuring reflectance at all collection angles. We already know the brightness at the specular position is B_{max}. The diffuse reflection is the integral on all angle configurations of the brightness. Hence Hunter's specular gloss G using the notation defined in this study is

$$G = \frac{B_{max}}{\iint B(\Phi_{inc}, \Phi_{col})\, d\Phi_{inc}\, d\Phi_{col}}. \quad \text{(B 9)}$$

The integral of brightness for every angle configurations is $B_{max}\gamma^*_B\sqrt{2\pi}$ (integral of the normal with maximum B_{max} and standard deviation γ^*_B), which gives

$$G = \frac{1}{\gamma^*_B\sqrt{2\pi}} = \frac{1}{2\gamma_B\sqrt{2\pi}}. \quad \text{(B 10)}$$

However, this is assuming the measurement of B_{max} was actually done at the normal to the multilayer $(\Phi_{inc} + \Phi_{col})/2 = t$. But there is no way to know whether it is the case without doing several goniometer measurements with different normal positions. Once this is done, γ_B can be estimated without doing additional integrating sphere measurements.

B.4.3. Difference/quotient between maximum and another position with the same span

Some studies [84,86,111] use the difference or the quotient between the brightness at the fibre position where it is maximum and another position. With this approach, they find t and B_{max}.

The difference or the quotient between these two positions can easily be linked to γ_B because we know that $B(\Phi_{inc}, \Phi_{col})$ is a normal function of parameters t and γ_B.

However, this is very sensitive to noise and measurement error because B_{max} and t are estimated with only one data point and γ_B (or its equivalent variable) with only two data points.

Appendix C. Structural colours with pigmentary component

The framework we presented here focuses on purely structural iridescent colours. However many colours integrate both pigmentary and structural components [147,148]. If there is a pigmentary component, it adds constant term B_{pigment} to brightness B:

$$B(\Phi_{\text{inc}}, \Phi_{\text{col}}) = B_{\text{irid}} + B_{\text{pigment}} \tag{C 1}$$

and

$$B(\Phi_{\text{inc}}, \Phi_{\text{col}}) = B_{\max} \exp - \frac{((\Phi_{\text{inc}} - \Phi_{\text{col}})/2 - t)^2}{2\gamma_B^2} + B_{\text{pigment}}. \tag{C 2}$$

This can easily be investigated using our protocol and statistical framework. The only difference is that four parameters ($B_{\max}$, t, γ_B and B_{pigment}) instead of three need to be estimated by running a nonlinear regression on equation (C 2) instead of equation (A 4).

There are cases where the structural and pigmentary components of colour act on very different regions of the light spectrum. This happens, for example, in *Colias eurytheme* [62], where iridescence is restricted to the UV region while the visible region colour is caused by pigments. In this case, our method can be applied directly by restricting the studied wavelength range to the region of interest (this option is available in the code provided in the electronic supplementary material).

References

1. Maynard Smith J, Harper DA 2009 *Animal signals*. Oxford Series in Ecology and Evolution. Oxford, UK: Oxford University Press.
2. Parker AR. 2000 515 million years of structural colour. *J. Opt. A: Pure Appl. Opt.* **2**, R15–R28. (doi:10.1088/1464-4258/2/6/201)
3. Bennett ATD, Cuthill IC, Partridge JC, Lunau K. 1997 Ultraviolet plumage colors predict mate preferences in starlings. *Proc. Natl Acad. Sci. USA* **94**, 8618–8621. (doi:10.1073/pnas.94.16.8618)
4. Perrier C, de Lope F, Møller AP, Ninni P. 2002 Structural coloration and sexual selection in the barn swallow *Hirundo rustica*. *Behav. Ecol.* **13**, 728–736. (doi:10.1093/beheco/13.6.728)
5. Doucet SM, Montgomerie R. 2003 Multiple sexual ornaments in satin bowerbirds: ultraviolet plumage and bowers signal different aspects of male quality. *Behav. Ecol.* **14**, 503–509. (doi:10.1093/beheco/arg035)
6. Doucet SM, Montgomerie R. 2003 Structural plumage colour and parasites in satin bowerbirds *Ptilonorhynchus violaceus*: implications for sexual selection. *J. Avian Biol.* **34**, 237–242. (doi:10.1034/j.1600-048X.2003.03113.x)
7. Zi J, Yu X, Li Y, Hu X, Xu C, Wang X, Liu X, Fu R. 2003 Coloration strategies in peacock feathers. *Proc. Natl Acad. Sci. USA* **100**, 12 576–12 578. (doi:10.1073/pnas.2133313100)
8. McGraw KJ. 2004 Multiple UV reflectance peaks in the iridescent neck feathers of pigeons. *Naturwissenschaften* **91**, 125–129. (doi:10.1007/s00114-003-0498-0)
9. Costa FJV, Macedo RH. 2005 Coccidian oocyst parasitism in the blue-black grassquit: influence on secondary sex ornaments and body condition. *Anim. Behav.* **70**, 1401–1409. (doi:10.1016/j.anbehav.2005.03.024)
10. Hill GE, Doucet SM, Buchholz R. 2005 The effect of coccidial infection on iridescent plumage coloration in wild turkeys. *Anim. Behav.* **69**, 387–394. (doi:10.1016/j.anbehav.2004.03.013)
11. Komdeur J, Oorebeek M, van Overveld T, Cuthill IC. 2005 Mutual ornamentation, age, and reproductive performance in the European starling. *Behav. Ecol.* **16**, 805–817. (doi:10.1093/beheco/ari059)
12. Shawkey MD, Hauber ME, Estep LK, Hill GE. 2006 Evolutionary transitions and mechanisms of matte and iridescent plumage coloration in grackles and allies (Icteridae). *J. R. Soc. Interface* **3**, 777–786. (doi:10.1098/rsif.2006.0131)
13. Bitton P-P, O'Brien EL, Dawson RD. 2007 Plumage brightness and age predict extrapair fertilization success of male tree swallows, *Tachycineta bicolor*. *Anim. Behav.* **74**, 1777–1784. (doi:10.1016/j.anbehav.2007.03.018)
14. Bitton P-P, Dawson RD. 2008 Age-related differences in plumage characteristics of male tree swallows *Tachycineta bicolor*: hue and brightness signal different aspects of individual quality. *J. Avian Biol.* **39**, 446–452. (doi:10.1111/j.0908-8857.2008.04283.x)
15. Bitton P-P, Dawson RD, Ochs CL. 2008 Plumage characteristics, reproductive investment and assortative mating in tree swallows *Tachycineta bicolor*. *Behav. Ecol. Sociobiol.* **62**, 1543–1550. (doi:10.1007/s00265-008-0583-7)
16. Galván I, Møller AP. 2009 Different roles of natural and sexual selection on senescence of plumage colour in the barn swallow. *Funct. Ecol.* **23**, 302–309. (doi:10.1111/j.1365-2435.2008.01504.x)
17. Eliason CM, Shawkey MD. 2010 Rapid, reversible response of iridescent feather color to ambient humidity. *Opt. Express* **18**, 21 284–21 292. (doi:10.1364/OE.18.021284)
18. Legagneux P, Théry M, Guillemain M, Gomez D, Bretagnolle V. 2010 Condition dependence of iridescent wing flash-marks in two species of dabbling ducks. *Behav. Processes* **83**, 324–330. (doi:10.1016/j.beproc.2010.01.017)
19. Maia R, Macedo RH. 2011 Achieving luster: prenuptial molt pattern predicts iridescent structural coloration in blue-black grassquits. *J. Ornithol.* **152**, 243–252. (doi:10.1007/s10336-010-0576-y)
20. Savard J-F, Keagy J, Borgia G. 2011 Blue, not UV, plumage color is important in satin bowerbird *Ptilonorhynchus violaceus* display. *J. Avian Biol.* **42**, 80–84. (doi:10.1111/j.1600-048X.2010.05128.x)
21. Eliason CM, Shawkey MD. 2011 Decreased hydrophobicity of iridescent feathers: a potential cost of shiny plumage. *J. Exp. Biol.* **214**, 2157–2163. (doi:10.1242/jeb.055822)
22. Lee E, Miyazaki J, Yoshioka S, Lee H, Sugita S. 2012 The weak iridescent feather color in the jungle crow *Corvus macrorhynchos*. *Ornithol. Sci.* **11**, 59–64. (doi:10.2326/osj.11.59)
23. Legagneux P, Clark RG, Guillemain M, Eraud C, Théry M, Bretagnolle V. 2012 Large-scale geographic variation in iridescent structural ornaments of a long-distance migratory bird. *J. Avian Biol.* **43**, 355–361. (doi:10.1111/j.1600-048X.2012.05666.x)
24. Maia R, Rubenstein DR, Shawkey MD. 2013 Key ornamental innovations facilitate diversification in an avian radiation. *Proc. Natl Acad. Sci. USA* **110**, 10 687–10 692. (doi:10.1073/pnas.1220784110)
25. Leclaire S, Pierret P, Chatelain M, Gasparini J. 2014 Feather bacterial load affects plumage condition, iridescent color, and investment in preening in pigeons. *Behav. Ecol.* **25**, 1192–1198. (doi:10.1093/beheco/aru109)
26. Eliason CM, Maia R, Shawkey MD. 2015 Modular color evolution facilitated by a complex nanostructure in birds. *Evolution* **69**, 357–367. (doi:10.1111/evo.12575)
27. Lee C-C, Liao S-F, Vukusic P. 2015 Measuring and modelling the reflectance spectra of male Swinhoe's pheasant feather barbules. *J. R. Soc. Interface* **12**, 20141354. (doi:10.1098/rsif.2014.1354)
28. Mahapatra BB, Marathe SA, Meyer-Rochow VB, Mishra M. 2016 A closer look at the feather coloration in the male purple sunbird, *Nectarinia asiatica*. *Micron* **85**, 44–50. (doi:10.1016/j.micron.2016.04.001)
29. Maia R, Rubenstein DR, Shawkey MD. 2016 Selection, constraint, and the evolution of coloration in African starlings. *Evolution* **70**, 1064–1079. (doi:10.1111/evo.12912)

30. Nam H-Y, Lee S-I, Lee J, Choi C-Y, Choe JC. 2016 Multiple structural colors of the plumage reflect age, sex, and territory ownership in the Eurasian magpie *Pica pica*. *Acta Ornithol.* **51**, 83–92. (doi:10.3161/00016454AO2016.51.1.007)
31. Ornelas JF, González C, Hernández-Baños BE, García-Moreno J. 2016 Molecular and iridescent feather reflectance data reveal recent genetic diversification and phenotypic differentiation in a cloud forest hummingbird. *Ecol. Evol.* **6**, 1104–1127. (doi:10.1002/ece3.1950)
32. Vaquero-Alba I, McGowan A, Pincheira-Donoso D, Evans MR, Dall SRX. 2016 A quantitative analysis of objective feather color assessment: measurements in the laboratory do not reflect true plumage color. *Auk* **133**, 325–337. (doi:10.1642/AUK-16-19.1)
33. Quinard A, Cézilly F, Motreuil S, Rossi J-M, Biard C. 2017 Reduced sexual dichromatism, mutual ornamentation, and individual quality in the monogamous Zenaida dove *Zenaida aurita*. *J. Avian Biol.* **48**, 489–501. (doi:10.1111/jav.00902)
34. Mossakowski D. 1979 Reflection measurements used in the analysis of structural colours of beetles. *J. Microsc.* **116**, 351–364. (doi:10.1111/j.1365-2818.1979.tb00220.x)
35. Schultz TD, Rankin MA. 1985 The ultrastructure of the epicuticular interference reflectors of tiger beetles (*Cicindela*). *J. Exp. Biol.* **117**, 87–110.
36. Chae J, Nishida S. 1999 Spectral patterns of the iridescence in the males of *Sapphirina* (Copepoda: Poecilostomatoida). *J. Mar. Biol. Assoc. UK* **79**, 437–443. (doi:10.1017/S0025315498000563)
37. Tada H, Mann SE, Miaoulis IN, Wong PY. 1999 Effects of a butterfly scale microstructure on the iridescent color observed at different angles. *Opt. Express* **5**, 87–92. (doi:10.1364/OE.5.000087)
38. Vukusic P, Sambles R, Lawrence C, Wakely G. 2001 Sculpted-multilayer optical effects in two species of *Papilio* butterfly. *Appl. Opt.* **40**, 1116–1125. (doi:10.1364/AO.40.001116)
39. Hariyama T, Takaku Y, Hironaka M, Horiguchi H, Komiya Y, Kurachi M. 2002 The origin of the iridescent colors in coleopteran elytron. *Forma* **17**, 123–132.
40. Kurachi M, Takaku Y, Komiya Y, Hariyama T. 2002 The origin of extensive colour polymorphism in *Plateumaris sericea* (Chrysomelidae, Coleoptera). *Naturwissenschaften* **89**, 295–298. (doi:10.1007/s00114-002-0332-0)
41. Liu F, Dong BQ, Liu XH, Zheng YM, Zi J. 2009 Structural color change in longhorn beetles *Tmesisternus isabellae*. *Opt. Express* **17**, 16183–16191. (doi:10.1364/OE.17.016183)
42. Schultz TD, Fincke OM. 2009 Structural colours create a flashing cue for sexual recognition and male quality in a Neotropical giant damselfly. *Funct. Ecol.* **23**, 724–732. (doi:10.1111/j.1365-2435.2009.01584.x)
43. Ingram AL, Deparis O, Boulenguez J, Kennaway G, Berthier S, Parker AR. 2011 Structural origin of the green iridescence on the chelicerae of the red-backed jumping spider, *Phidippus johnsoni* (Salticidae: Araneae). *Arthrop. Struct. Dev.* **40**, 21–25. (doi:10.1016/j.asd.2010.07.006)
44. Kuitunen K, Gorb SN. 2011 Effects of cuticle structure and crystalline wax coverage on the coloration in young and old males of *Calopteryx splendens* and *Calopteryx virgo*. *Zoology* **114**, 129–139. (doi:10.1016/j.zool.2011.01.003)
45. Gur D, Leshem B, Farstey V, Oron D, Addadi L, Weiner S. 2016 Light-induced color change in the sapphirinid copepods: tunable photonic crystals. *Adv. Funct. Mater.* **26**, 1393–1399. (doi:10.1002/adfm.201504339)
46. Wilts BD, Giraldo MA, Stavenga DG. 2016 Unique wing scale photonics of male Rajah Brooke's birdwing butterflies. *Front. Zool.* **13**, 36. (doi:10.1186/s12983-016-0168-7)
47. Onelli OD, van de Kamp T, Skepper JN, Powell J, Rolo TDS, Baumbach T, Vignolini S. 2017 Development of structural colour in leaf beetles. *Sci. Rep.* **7**, 1373. (doi:10.1038/s41598-017-01496-8)
48. Trzeciak TM, Wilts BD, Stavenga DG, Vukusic P. 2012 Variable multilayer reflection together with long-pass filtering pigment determines the wing coloration of papilionid butterflies of the nireus group. *Opt. Express* **20**, 8877–8890. (doi:10.1364/OE.20.008877)
49. Gur D, Leshem B, Oron D, Weiner S, Addadi L. 2014 The structural basis for enhanced silver reflectance in koi fish scale and skin. *J. Am. Chem. Soc.* **136**, 17 236–17 242. (doi:10.1021/ja509340c)
50. Snyder HK, Maia R, D'Alba L, Shultz AJ, Rowe KMC, Rowe KC, Shawkey MD. 2012 Iridescent colour production in hairs of blind golden moles (Chrysochloridae). *Biol. Lett.* **8**, 393–396. (doi:10.1098/rsbl.2011.1168)
51. Lee DW. 1991 Ultrastructural basis and function of iridescent blue colour of fruits in *Elaeocarpus*. *Nature* **349**, 260–262. (doi:10.1038/349260a0)
52. Lee DW, Taylor GT, Irvine AK. 2000 Structural fruit coloration in *Delarbrea michieana* (Araliaceae). *Int. J. Plant Sci.* **161**, 297–300. (doi:10.1086/314249)
53. Vignolini S, Rudall PJ, Rowland AV, Reed A, Moyroud E, Faden RB, Baumberg JJ, Glover BJ, Steiner U. 2012 Pointillist structural color in Pollia fruit. *Proc. Natl Acad. Sci. USA* **109**, 15 712–15 715. (doi:10.1073/pnas.1210105109)
54. Chandler CJ, Wilts BD, Vignolini S, Brodie J, Steiner U, Rudall PJ, Glover BJ, Gregory T, Walker RH. 2015 Structural colour in *Chondrus crispus*. *Sci. Rep.* **5**, 11645. (doi:10.1038/srep11645)
55. Huxley J. 1975 The basis of structural colour variation in two species of *Papilio*. *J. Entomol. Ser. A Gen. Entomol.* **50**, 9–22. (doi:10.1111/j.1365-3032.1975.tb00087.x)
56. Kemp DJ. 2006 Heightened phenotypic variation and age-based fading of ultraviolet butterfly wing coloration. *Evol. Ecol. Res.* **8**, 515–527.
57. Papke RS, Kemp DJ, Rutowski RL. 2007 Multimodal signalling: structural ultraviolet reflectance predicts male mating success better than pheromones in the butterfly *Colias eurytheme* L. (Pieridae). *Anim. Behav.* **73**, 47–54. (doi:10.1016/j.anbehav.2006.07.004)
58. Pegram KV, Nahm AC, Rutowski RL, Todd S. 2013 Warning color changes in response to food deprivation in the pipevine swallowtail butterfly, *Battus philenor*. *J. Insect Sci.* **13**, 1–16. (doi:10.1673/031.013.11001)
59. Kemp DJ, Jones D, Macedonia JM, Krockenberger AK. 2014 Female mating preferences and male signal variation in iridescent *Hypolimnas* butterflies. *Anim. Behav.* **87**, 221–229. (doi:10.1016/j.anbehav.2013.11.001)
60. Thurman TJ, Seymoure BM. 2016 A bird's eye view of two mimetic tropical butterflies: coloration matches predator's sensitivity. *J. Zool.* **298**, 159–168. (doi:10.1111/jzo.12305)
61. Parra JL. 2010 Color evolution in the hummingbird genus *Coeligena*. *Evolution* **64**, 324–335. (doi:10.1111/j.1558-5646.2009.00827.x)
62. Rutowski RL, Macedonia JM, Morehouse NI, Taylor-Taft L. 2005 Pterin pigments amplify iridescent ultraviolet signal in males of the orange sulphur butterfly, *Colias eurytheme*. *Proc. R. Soc. B* **272**, 2329–2335. (doi:10.1098/rspb.2005.3216)
63. Rutowski RL, Macedonia JM, Kemp DJ, Taylor-Taft L. 2007 Diversity in structural ultraviolet coloration among female sulphur butterflies (Coliadinae, Pieridae). *Arthrop. Struct. Dev.* **36**, 280–290. (doi:10.1016/j.asd.2006.11.005)
64. Imafuku M, Ogihara N. 2016 Wing scale orientation alters reflection directions in the green hairstreak *Chrysozephyrus smaragdinus* (Lycaenidae; Lepidoptera). *Zool. Sci.* **33**, 616–622. (doi:10.2108/zs160041)
65. Kientz B, Ducret A, Luke S, Vukusic P, Mignot T, Rosenfeld E. 2012 Glitter-like iridescence within the Bacteroidetes especially *Cellulophaga spp.*: optical properties and correlation with gliding motility. *PLoS ONE* **7**, e52900. (doi:10.1371/journal.pone.0052900)
66. Dakin R, Montgomerie R. 2013 Eye for an eyespot: how iridescent plumage ocelli influence peacock mating success. *Behav. Ecol.* **24**, 1048–1057. (doi:10.1093/beheco/art045)
67. Berthier S, Charron E, Boulenguez J. 2006 Morphological structure and optical properties of the wings of Morphidae. *Insect Sci.* **13**, 145–158. (doi:10.1111/j.1744-7917.2006.00077.x)
68. Doucet SM, Shawkey MD, Hill GE, Montgomerie R. 2006 Iridescent plumage in satin bowerbirds: structure, mechanisms and nanostructural predictors of individual variation in colour. *J. Exp. Biol.* **209**, 380–390. (doi:10.1242/jeb.01988)
69. Yin H *et al.* 2006 Iridescence in the neck feathers of domestic pigeons. *Phys. Rev. E* **74**, 051916. (doi:10.1103/PhysRevE.74.051916)
70. Yoshioka S, Nakamura E, Kinoshita S. 2007 Origin of two-color iridescence in rock dove's feather. *J. Phys. Soc. Jpn.* **76**, 013801. (doi:10.1143/JPSJ.76.013801)
71. Maia R, Caetano JAV, Báo SN, Macedo RH. 2009 Iridescent structural colour production in male blue-black grassquit feather barbules: the role of keratin and melanin. *J. R. Soc. Interface* **6**, S203–S211. (doi:10.1098/rsif.2008.0460.focus)
72. Shawkey MD, D'Alba L, Wozny J, Eliason C, Koop JAH, Jia L. 2011 Structural color change following

hydration and dehydration of iridescent mourning dove (*Zenaida macroura*) feathers. *Zoology* **114**, 59–68. (doi:10.1016/j.zool.2010.11.001)

73. Yoshioka S, Kinoshita S. 2011 Direct determination of the refractive index of natural multilayer systems. *Phys. Rev. E* **83**, 051917. (doi:10.1103/PhysRevE.83.051917)
74. Wilts BD, Michielsen K, Raedt HD, Stavenga DG. 2014 Sparkling feather reflections of a bird-of-paradise explained by finite-difference time-domain modeling. *Proc. Natl Acad. Sci. USA* **111**, 4363–4368. (doi:10.1073/pnas.1323611111)
75. Igic B *et al.* 2015 A nanostructural basis for gloss of avian eggshells. *J. R. Soc. Interface* **12**, 20141210. (doi:10.1098/rsif.2014.1210)
76. Stavenga DG, Leertouwer HL, Osorio DC, Wilts BD. 2015 High refractive index of melanin in shiny occipital feathers of a bird of paradise. *Light: Sci. Appl.* **4**, e243. (doi:10.1038/lsa.2015.16)
77. Stavenga DG, Leertouwer HL, Wilts BD. 2018 Magnificent magpie colours by feathers with layers of hollow melanosomes. *J. Exp. Biol.* **221**, jeb174656. (doi:10.1242/jeb.174656)
78. Stavenga DG, van der Kooi CJ, Wilts BD. 2017 Structural coloured feathers of mallards act by simple multilayer photonics. *J. R. Soc. Interface* **14**, 20170407. (doi:10.1098/rsif.2017.0407)
79. Vukusic P, Wootton RJ, Sambles JR. 2004 Remarkable iridescence in the hindwings of the damselfly *Neurobasis chinensis chinensis* (Linnaeus) (Zygoptera: Calopterygidae). *Proc. R. Soc. Lond. B* **271**, 595–601. (doi:10.1098/rspb.2003.2595)
80. Wickham S, Large MCJ, Poladian L, Jermiin LS. 2006 Exaggeration and suppression of iridescence: the evolution of two-dimensional butterfly structural colours. *J. R. Soc. Interface* **3**, 99–109. (doi:10.1098/rsif.2005.0071)
81. Stavenga DG, Giraldo MA, Leertouwer HL. 2010 Butterfly wing colors: glass scales of *Graphium sarpedon* cause polarized iridescence and enhance blue/green pigment coloration of the wing membrane. *J. Exp. Biol.* **213**, 1731–1739. (doi:10.1242/jeb.041434)
82. Yoshioka S, Kinoshita S, Iida H, Hariyama T. 2012 Phase-adjusting layers in the multilayer reflector of a jewel beetle. *J. Phys. Soc. Jpn.* **81**, 054801. (doi:10.1143/JPSJ.81.054801)
83. Mouchet SR, Lobet M, Kolaric B, Kaczmarek AM, Van Deun R, Vukusic P, Deparis O, Van Hooijdonk E. 2017 Photonic scales of *Hoplia coerulea* beetle: any colour you like. *Mater. Tod. Proc.* **4**, 4979–4986. (doi:10.1016/j.matpr.2017.04.104)
84. Meadows MG, Roudybush TE, McGraw KJ. 2012 Dietary protein level affects iridescent coloration in Anna's hummingbirds, *Calypte anna*. *J. Exp. Biol.* **215**, 2742–2750. (doi:10.1242/jeb.069351)
85. Van Wijk S, Bourret A, Bélisle M, Garant D, Pelletier F. 2016 The influence of iridescent coloration directionality on male tree swallows' reproductive success at different breeding densities. *Behav. Ecol. Sociobiol.* **70**, 1557–1569. (doi:10.1007/s00265-016-2164-5)
86. Van Wijk S, Bélisle M, Garant D, Pelletier F. 2016 A reliable technique to quantify the individual variability of iridescent coloration in birds. *J. Avian Biol.* **47**, 227–234. (doi:10.1111/jav.00750)
87. Simpson RK, McGraw KJ. 2018 It's not just what you have, but how you use it: solar-positional and behavioural effects on hummingbird colour appearance during courtship. *Ecol. Lett.* **21**, 1413–1422. (doi:10.1111/ele.13125)
88. Kemp DJ, Vukusic P, Rutowski RL. 2006 Stress-mediated covariance between nano-structural architecture and ultraviolet butterfly coloration. *Funct. Ecol.* **20**, 282–289. (doi:10.1111/j.1365-2435.2006.01100.x)
89. Kemp DJ, Rutowski RL. 2007 Condition dependence, quantitative genetics, and the potential signal content of iridescent ultraviolet butterfly coloration. *Evolution* **61**, 168–183. (doi:10.1111/j.1558-5646.2007.00014.x)
90. Rutowski RL, Macedonia JM, Merry JW, Morehouse NI, Yturralde K, Taylor-Taft L, Gaalema D, Kemp DJ, Papke RS. 2007 Iridescent ultraviolet signal in the orange sulphur butterfly (*Colias eurytheme*): spatial, temporal and spectral properties. *Biol. J. Linnean Soc.* **90**, 349–364. (doi:10.1111/j.1095-8312.2007.00749.x)
91. Kemp DJ, Macedonia JM, Ball TS, Rutowski RL. 2008 Potential direct fitness consequences of ornament-based mate choice in a butterfly. *Behav. Ecol. Sociobiol.* **62**, 1017–1026. (doi:10.1007/s00265-007-0529-5)
92. Kemp DJ. 2008 Female mating biases for bright ultraviolet iridescence in the butterfly *Eurema hecabe* (Pieridae). *Behav. Ecol.* **19**, 1–8. (doi:10.1093/beheco/arm094)
93. Ghate E, Bhoraskar SV, Kulkarni GR. 2013 Study of nano-architecture of the wings of *Paris Peacock* butterfly. *Proc. SPIE* **8598**, 859805. (doi:10.1117/12.2003061)
94. Gur D, Leshem B, Pierantoni M, Farstey V, Oron D, Weiner S, Addadi L. 2015 Structural basis for the brilliant colors of the sapphirinid copepods. *J. Am. Chem. Soc.* **137**, 8408–8411. (doi:10.1021/jacs.5b05289)
95. Piszter G, Kertész K, Bálint Z, Biró LP. 2016 Variability of the structural coloration in two butterfly species with different prezygotic mating strategies. *PLoS ONE* **11**, e0165857. (doi:10.1371/journal.pone.0165857)
96. Parnell AJ *et al.* 2018 Wing scale ultrastructure underlying convergent and divergent iridescent colours in mimetic *Heliconius* butterflies. *J. R. Soc. Interface* **15**, 20170948. (doi:10.1098/rsif.2017.0948)
97. Mäthger LM, Land MF, Siebeck UE, Marshall NJ. 2003 Rapid colour changes in multilayer reflecting stripes in the paradise whiptail, *Pentapodus paradiseus*. *J. Exp. Biol.* **206**, 3607–3613. (doi:10.1242/jeb.00599)
98. i de Lanuza GP, Font E. 2014 Now you see me, now you don't: iridescence increases the efficacy of lizard chromatic signals. *Naturwissenschaften* **101**, 831–837. (doi:10.1007/s00114-014-1224-9)
99. i de Lanuza GP, Font E. 2016 Iridescent (angle-dependent reflectance) properties of dorsal coloration in *Podarcis muralis* (Laurenti, 1768). *Amphibia-Reptilia* **37**, 441–445.
100. Santos SI, Lumeij JT, Westers P, van Wandelen BB. 2007 Sexual dichromatism in the European magpie *Pica pica*. Not as black and white as expected. *Ardea* **95**, 299–310. (doi:10.5253/078.095.0212)
101. Plattner L. 2004 Optical properties of the scales of *Morpho rhetenor* butterflies: theoretical and experimental investigation of the back-scattering of light in the visible spectrum. *J. R. Soc. Interface* **1**, 49–59. (doi:10.1098/rsif.2004.0006)
102. Pirih P, Wilts BD, Stavenga DG. 2011 Spatial reflection patterns of iridescent wings of male pierid butterflies: curved scales reflect at a wider angle than flat scales. *J. Comp. Physiol. A* **197**, 987–997. (doi:10.1007/s00359-011-0661-6)
103. Kientz B, Luke S, Vukusic P, Péteri R, Beaudry C, Renault T, Simon D, Mignot T, Rosenfeld E. 2016 A unique self-organization of bacterial sub-communities creates iridescence in *Cellulophaga lytica* colony biofilms. *Sci. Rep.* **6**, 19906. (doi:10.1038/srep19906)
104. Eliason CM, Shawkey MD. 2012 A photonic heterostructure produces diverse iridescent colours in duck wing patches. *J. R. Soc. Interface* **9**, 2279–2289. (doi:10.1098/rsif.2012.0118)
105. Madsen V, Dabelsteen T, Osorio D, Osorno JL. 2007 Morphology and ornamentation in male magnificent frigatebirds: variation with age class and mating status. *Am. Nat.* **169**, S93–S111. (doi:10.1086/510096)
106. Liu F, Yin H, Dong B, Qing Y, Zhao L, Meyer S, Liu X, Zi J, Chen B. 2008 Inconspicuous structural coloration in the elytra of beetles *Chlorophila obscuripennis* (Coleoptera). *Phys. Rev. E* **77**, 012901. (doi:10.1103/PhysRevE.77.012901)
107. Stavenga DG, Wilts BD, Leertouwer HL, Hariyama T. 2011 Polarized iridescence of the multilayered elytra of the Japanese jewel beetle, *Chrysochroa fulgidissima*. *Phil. Trans. R. Soc. B* **366**, 709–723. (doi:10.1098/rstb.2010.0197)
108. Johansen VE, Catón L, Hamidjaja R, Oosterink E, Wilts BD, Rasmussen TS, Sherlock MM, Ingham CJ, Vignolini S. 2018 Genetic manipulation of structural color in bacterial colonies. *Proc. Natl Acad. Sci. USA* **115**, 2652–2657. (doi:10.1073/pnas.1716214115)
109. Edo S, Okoshi K, Kang S, Tokita M, Watanabe J. 2010 Unique reflection property due to bumpy multilayer structure in elytra of *Rhomborrhina unicolor*. *Jpn J. Appl. Phys.* **49**, 047201. (doi:10.1143/JJAP.49.047201)
110. Osorio DC, Ham AD. 2002 Spectral reflectance and directional properties of structural coloration in bird plumage. *J. Exp. Biol.* **205**, 2017–2027.
111. Loyau A, Gomez D, Moureau B, Théry M, Hart NS, Jalme MS, Bennett ATD, Sorci G. 2007 Iridescent structurally based coloration of eyespots correlates with mating success in the peacock. *Behav. Ecol.* **18**, 1123–1131. (doi:10.1093/beheco/arm088)
112. White TE, Zeil J, Kemp DJ. 2015 Signal design and courtship presentation coincide for highly biased

delivery of an iridescent butterfly mating signal. *Evolution* **69**, 14–25. (doi:10.1111/evo.12551)

113. Brink DJ, van der Berg NG. 2004 Structural colours from the feathers of the bird *Bostrychia hagedash*. *J. Phys. D: Appl. Phys.* **37**, 813–818. (doi:10.1088/0022-3727/37/5/025)
114. Meadows MG, Morehouse NI, Rutowski RL, Douglas JM, McGraw KJ. 2011 Quantifying iridescent coloration in animals: a method for improving repeatability. *Behav. Ecol. Sociobiol.* **65**, 1317–1327. (doi:10.1007/s00265-010-1135-5)
115. Stavenga DG, Leertouwer HL, Marshall NJ, Osorio DC. 2011 Dramatic colour changes in a bird of paradise caused by uniquely structured breast feather barbules. *Proc. R. Soc. B* **278**, 2098–2104. (doi:10.1098/rspb.2010.2293)
116. Rutowski RL, Nahm AC, Macedonia JM. 2010 Iridescent hindwing patches in the pipevine swallowtail: differences in dorsal and ventral surfaces relate to signal function and context. *Funct. Ecol.* **24**, 767–775. (doi:10.1111/j.1365-2435.2010.01693.x)
117. Rutowski RL, Rajyaguru PK. 2013 Male-specific iridescent coloration in the pipevine swallowtail (*Battus philenor*) is used in mate choice by females but not sexual discrimination by males. *J. Insect Behav.* **26**, 200–211. (doi:10.1007/s10905-012-9348-2)
118. Waldron SJ, Endler JA, Valkonen JK, Honma A, Dobler S, Mappes J. 2017 Experimental evidence suggests that specular reflectance and glossy appearance help amplify warning signals. *Sci. Rep.* **7**, 257. (doi:10.1038/s41598-017-00217-5)
119. Brink DJ, van der Berg NG, Botha AJ. 2002 Iridescent colors on seashells: an optical and structural investigation of *Helcion pruinosus*. *Appl. Opt.* **41**, 717–722. (doi:10.1364/AO.41.000717)
120. Noh H, Liew SF, Saranathan V, Prum RO, Mochrie SGJ, Dufresne ER, Cao H. 2010 Contribution of double scattering to structural coloration in quasiordered nanostructures of bird feathers. *Phys. Rev. E* **81**, 051923. (doi:10.1103/PhysRevE.81.051923)
121. Eliason CM, Bitton P-P, Shawkey MD. 2013 How hollow melanosomes affect iridescent colour production in birds. *Proc. R. Soc. B* **280**, 20131505. (doi:10.1098/rspb.2013.1505)
122. Wilts BD, Pirih P, Arikawa K, Stavenga DG. 2013 Shiny wing scales cause spec(tac)ular camouflage of the angled sunbeam butterfly, *Curetis acuta*. *Biol. J. Linnean Soc.* **109**, 279–289. (doi:10.1111/bij.12070)
123. Doucet SM, Meadows MG. 2009 Iridescence: a functional perspective. *J. R. Soc. Interface* **6**(Suppl. 2), S115–S132. (doi:10.1098/rsif.2008.0395.focus)
124. Simpson RK, McGraw KJ. 2018 Two ways to display: male hummingbirds show different color-display tactics based on sun orientation. *Behav. Ecol.* **29**, 637–648. (doi:10.1093/beheco/ary016)
125. Moyroud E *et al.* 2017 Disorder in convergent floral nanostructures enhances signalling to bees. *Nature* **550**, 469–474. (doi:10.1038/nature24285)
126. Montgomerie R. 2006 Analyzing colors. In *Bird coloration, volume 1: mechanisms and measurements* (eds GE Hill, KJ McGraw), p. 640. Cambridge, MA: Harvard University Press.
127. Gur D, Palmer BA, Leshem B, Oron D, Fratzl P, Weiner S, Addadi L. 2015 The mechanism of color change in the neon tetra fish: a light-induced tunable photonic crystal array. *Angew. Chem. Int. Ed.* **54**, 12426–12430. (doi:10.1002/anie.201502268)
128. Land MF. 1966 A multilayer interference reflector in the eye of the scallop, *Pecten maximus*. *J. Exp. Biol.* **45**, 433–447.
129. Brink DJ, Lee ME. 1998 Thin-film biological reflectors: optical characterization of the *Chrysiridia croesus* moth. *Appl. Opt.* **37**, 4213–4217. (doi:10.1364/AO.37.004213)
130. Kinoshita S, Yoshioka S. 2005 Structural colors in nature: the role of regularity and irregularity in the structure. *ChemPhysChem* **6**, 1442–1459. (doi:10.1002/cphc.200500007)
131. Land MF. 1972 The physics and biology of animal reflectors. *Prog. Biophys. Mol. Biol.* **24**, 75–106. (doi:10.1016/0079-6107(72)90004-1)
132. Parker AR, McKenzie DR, Large MCJ. 1998 Multilayer reflectors in animals using green and gold beetles as contrasting examples. *J. Exp. Biol.* **201**, 1307–1313.
133. Kinoshita S, Yoshioka S, Miyazaki J. 2008 Physics of structural colors. *Rep. Prog. Phys.* **71**, 076401. (doi:10.1088/0034-4885/71/7/076401)
134. Vukusic P, Sambles JR, Lawrence CR, Wootton RJ. 2002 Limited-view iridescence in the butterfly *Ancyluris meliboeus*. *Proc. R. Soc. Lond. B* **269**, 7–14. (doi:10.1098/rspb.2001.1836)
135. Del Hoyo J, Elliott A, Sargatal J, Christie DA, de Juana E. 2017 Handbook of the Birds of the World Alive. See hbw.com.
136. McGuire JA, Witt CC, Remsen JVJ, Corl A, Rabosky DL, Altshuler DL, Dudley R. 2014 Molecular phylogenetics and the diversification of hummingbirds. *Curr. Biol.* **24**, 910–916. (doi:10.1016/j.cub.2014.03.016)
137. Berthier S. 2007 *Iridescences: the physical colors of insects*. New York, NY: Springer.
138. Chen D-M, Goldsmith TH. 1986 Four spectral classes of cone in the retinas of birds. *J. Comp. Physiol. A* **159**, 473–479. (doi:10.1007/BF00604167)
139. Maia R, Eliason CM, Bitton P-P, Doucet SM, Shawkey MD. 2013 Pavo: an R package for the analysis, visualization and organization of spectral data. *Methods Ecol. Evol.* **4**, 906–913. (doi:10.1111/2041-210X.12069)
140. Nakagawa S, Schielzeth H. 2010 Repeatability for Gaussian and non-Gaussian data: a practical guide for biologists. *Biol. Rev.* **85**, 935–956. (doi:10.1111/j.1469-185X.2010.00141.x)
141. Evans SR, Hinks AE, Wilkin TA, Sheldon BC. 2010 Age, sex and beauty: methodological dependence of age- and sex-dichromatism in the great tit *Parus major*. *Biol. J. Linnean Soc.* **101**, 777–796. (doi:10.1111/j.1095-8312.2010.01548.x)
142. Midamegbe A, Grégoire A, Staszewski V, Perret P, Lambrechts MM, Boulinier T, Doutrelant C. 2013 Female blue tits with brighter yellow chests transfer more carotenoids to their eggs after an immune challenge. *Oecologia* **173**, 387–397. (doi:10.1007/s00442-013-2617-8)
143. Charmantier A, Wolak ME, Grégoire A, Fargevieille A, Doutrelant C. 2017 Colour ornamentation in the blue tit: quantitative genetic (co)variances across sexes. *Heredity* **118**, 125–134. (doi:10.1038/hdy.2016.70)
144. Maia R, D'Alba L, Shawkey MD. 2011 What makes a feather shine? A nanostructural basis for glossy black colours in feathers. *Proc. R. Soc. B* **278**, 1973–1980. (doi:10.1098/rspb.2010.1637)
145. Iskandar J-P, Eliason CM, Astrop T, Igic B, Maia R, Shawkey MD. 2016 Morphological basis of glossy red plumage colours. *Biol. J. Linnean Soc.* **119**, 477–487. (doi:10.1111/bij.12810)
146. Hunter RS. 1937 Methods of determining gloss. *J. Res. Natl Bureau Standards* **18**, 19–39. (doi:10.6028/jres.018.006)
147. Prum RO. 2006 Anatomy, physics, and evolution of structural colors. In *Bird coloration, volume 1: mechanisms and measurements* (eds GE Hill, KJ McGraw), p. 640. Cambridge, MA: Harvard University Press.
148. D'Alba L, Kieffer L, Shawkey MD. 2012 Relative contributions of pigments and biophotonic nanostructures to natural color production: a case study in budgerigar (*Melopsittacus undulatus*) feathers. *J. Exp. Biol.* **215**, 1272–1277. (doi:10.1242/jeb.064907)